Accepted Manuscript

International Journal of Applied Mechanics

Article Title:	Thermo-Mechanical Creep Analysis of FGM Thick Cylindrical Pressure Vessels with Variable Thickness
Author(s):	Mosayeb Davoudi Kashkoli, Khosro Naderan Tahan, Mohammad Zamani Nejad
DOI:	10.1142/S1758825118500084
Received:	29 September 2017
Accepted:	28 December 2017
To be cited as:	Mosayeb Davoudi Kashkoli, Khosro Naderan Tahan, Mohammad Zamani Nejad, Thermo-Mechanical Creep Analysis of FGM Thick Cylindrical Pressure Vessels with Variable Thickness, *International Journal of Applied Mechanics*, doi: 10.1142/S1758825118500084
Link to final version:	http://dx.doi.org/10.1142/S1758825118500084

World Scientific
www.worldscientific.com

Thermo-Mechanical Creep Analysis of FGM Thick Cylindrical Pressure Vessels with Variable Thickness

Mosayeb Davoudi Kashkoli and Khosro Naderan Tahan

Department of Mechanical Engineering, Shahid Chamran University of Ahvaz, Ahvaz, Iran

Mohammad Zamani Nejad[*]
Department of Mechanical Engineering, Yasouj University, Yasouj, Iran
m_zamani@yu.ac.ir , m.zamani.n@gmail.com

Received Day Month Year
Revised Day Month Year

In the present study, a theoretical solution for thermo- mechanical creep analysis of functionally graded (FG) thick cylindrical pressure vessel with variable thickness based on the first-order shear deformation theory (FSDT) and multi-layer method (MLM), is presented. To the best of the researchers' knowledge, in the literature, there is no study carried out into FSDT and MLM for creep response of cylindrical pressure vessels with variable thickness under thermal and mechanical loadings. The vessel is subjected to a temperature gradient and non-uniform internal pressure. All mechanical and thermal properties except Poisson's ratio are assumed to vary along the thickness direction based on a power function. The thermo-mechanical creep response of the material is described by Norton's law. The virtual work principle is applied to extract the non-homogeneous differential equations system with variable coefficients. Using, the MLM, these differential equations system is converted into a system of differential equations with constant coefficients. This set of differential equations is solved analytically by applying boundary and continuity conditions between the layers. In order to verify the results of this study, the finite element method (FEM) has been used and according to the results, good agreement has been achieved. It can be concluded that the temperature gradient has significant influence on the creep responses of FG thick cylindrical pressure vessel.

Keywords: Creep; cylindrical pressure vessel; functionally graded material (FGM); first-order shear deformation theory (FSDT); multi-layer method (MLM); variable thickness.

1. Introduction

Due to the high thermal and mechanical loading conditions in various industries, researchers proposed FGMs to be employed to fabricate structures that work in this conditions [Kordkheili and Livani, 2013]. In FGMs the mechanical properties vary smoothly and continuously from one surface to the other [Ghannad *et al.*, 2012; Dehghan *et al.*, 2016; Sofiyev and Kuruoğlu, 2016]. A number of papers considering various aspects of FGM have been published in recent years [Afshin *et al.*, 2017; Gharibi *et al.* 2017; Mazarei *et al.*, 2016; Sobhy, 2015; Nayebi *et al.*, 2015; Nejad and Rahimi, 2010; Nejad *et al.*, 2009].

Cylindrical shells are widely used in many engineering applications. In some of these applications, for instance in exteriors of rockets and missiles or pressure vessels, due to the variable pressure in longitudinal direction, the use of variable-thickness cylindrical shells

[*] Corresponding author.

is suggested as one of the ways to optimizing stress and weight. [Shariati *et al.*, 2015, Ghannad *et al.*, 2013]. There are many studies in the literature carried out into the analysis of cylindrical vessels under various assumptions and conditions [Fatehi and Nejad, 2014; Nejad and Fatehi, 2015; Nejad *et al.*, 2009]. The literature that addresses the creep stresses of thick cylindrical shells with variable thickness is quite limited.

Due to the high strength and thermal resistance properties, FGM cylindrical shells are used in advanced applications such as missiles, pressure vessels, tanks, gun barrels and other applications [Dung and Chan, 2017]. At high temperatures creep behavior usually occurs in the cylinders under thermo-mechanical loading, thereby affecting performance of the system. In order to better utilize the components used in these loading conditions, it is necessary to investigate the creep phenomenon to prevent sudden damages. In other words, life assessment of such components is very important because failures of these components are always catastrophic. Several analytical and numerical formulations to model the behavior of single and multilayered structures are available in the literature. Among them, the classical FSDT based on Reissner and Mindlin, assume constant transverse shear stresses in the thickness direction [Mantari and Granados, 2015]. Using this method, several problems with different conditions such as geometries, loadings and boundary conditions could be more easily solved by this method. A number of papers considering various aspects of vessels have been investigated using FSDT and also the higher-order shear deformation theories (HSDT) [Jabbari *et al.*, 2015; Nejad *et al.*, 2015b; Nejad *et al.*, 2015c; Ghannad and Nejad, 2010; Jabbari *et al.*, 2016; Sofiyev, 2016; Kashkoli *et al.*, 2017; Nejad *et al.*, 2017a; Nejad *et al.*, 2017b; Sofiyev *et al.*, 2017a; Sofiyev *et al.*, 2017b; Ghannad *et al.* 2009].

It is necessary to study the creep behavior of high temperature metals and researchers study the ways to improve the high-temperature strength of metals. Mechanical-thermal treatment (MTT) is one of ways to do this. According to experimental data, preliminary MTT considerably increases the high-temperature strength of metals, namely, the steady state creep rate of metals [Rusinko, 2013]. The material constitutive models and the solution methods for creep problems are important and discussed in [Kassner, 2015]. A summary of creep laws for common engineering materials is provided in [Naumenko and Altenbach, 2007]. Most of these models describe the secondary creep stage in uniaxial tests with constant load/stress condition where creep rate is nearly constant. Bailey-Norton and Norton laws are the widespread creep constitutive models which is used by most of the researchers. Strain rates and equivalent stress are related to each other according to a power law function. Extensive studies have been carried out, both theoretically and numerically, on creep stress distribution in functionally gradient thick-walled pressure vessels under mechanical and thermal loadings [Loghman *et al.*, 2010; Daghigh *et al.*, 2013; Kordkheili and Livani, 2013; Fesharaki *et al.*, 2014; Kashkoli and Nejad, 2014; Nejad and Kashkoli, 2014; Loghman *et al.*, 2011; Kashkoli and Nejad, 2015; Kashkoli *et al.*, 2017a; Loghman and Moradi, 2017; Nejad *et al.*, 2015a].

The previous studies, theoretical solutions for creep response of thick cylindrical pressure vessels is based on the plane elasticity theory (PET) or classical theory in which the shear

stress τ_{rx} and shear strain γ_{rx}, are considered zero. Regarding the problems which could not be solved through PET, the solution based on the FSDT is suggested. At the boundary areas of a thick-walled cylinder with clamped-clamped, having variable thickness and non-uniform pressure, given that creep displacements and stresses are dependent on radius and length, use cannot be made of PET, and FSDT must be used. The shear stress in boundary areas cannot be ignored, but in areas further away from the boundaries, it can be ignored. Therefore, the PET can be used, provided that the shear strain is zero.

In the present study, for the first time, thermo-mechanical creep response of a thick cylindrical pressure vessel with variable thickness made of functionally graded material, such as stainless steel-zirconia is investigated using FSDT and MLM. The vessel is subjected to the non-uniform internal pressure and distributed temperature field due to steady-state heat conduction from inner to outer surface of the vessel. The governing equations which are a system of ordinary differential equations with variable coefficients have been derived using virtual work principle. Solving these equations is difficult and in some cases impossible. The MLM method, which is a semi-analytical method, is proposed to solve these equations. For this purpose, the FG cylindrical vessel is divided into n homogenous disks. With regard to the continuity between layers and applying boundary conditions, the governing set of differential equations with constant coefficients is solved. Therefore, the MLM converts the ordinary differential equations with variable coefficients into the differential equations with constant coefficients which have analytical solutions. The results obtained for creep stresses and displacements are compared with the solutions carried out through the FEM and good agreement was found between the results. The results of this study are applicable for designing optimum FG thick cylindrical vessel.

2. Basic formulations and solutions

In Fig. 1, the geometry of a thick axisymmetric cylinder with variable thickness is shown. The cylinder is subjected to non-uniform internal pressure *P* and a temperature gradient *T* due to steady state heat conduction in thickness of the cylinder. In Fig. 1, *h* and *L* are thickness and length of the cylinder respectively.

2.1. *Material properties*

In order to model the material properties of FGM in this study, the power low distribution which is the most commonly model in the literature, is used. In this model, it is assumed that the material properties graded continuously through the thickness according to the following power-law expression [Sofiyev, 2011]:

$$p(z) = (p_o - p_i)\left(\frac{1}{2} + \frac{z}{h}\right)^n + p_i \tag{1}$$

where p denotes one of the effective material properties, such as the modulus of elasticity E, density ρ, thermal conductivity k_T, or thermal expansion coefficient α, p_i and p_o

are the corresponding properties of the inner and outer surfaces of the cylinder respectively and n denotes a non-negative volume fraction exponent characterizing the distributions of material properties, called power-law index. The effect of Poisson's ratio v on deformation of the engineering materials, compared to other properties is small and ignorable, therefore in this study the Poisson's ratio is assumed as constant. For numerical results, there is considered stainless steel and zirconia FG cylinder. Fig. 2 shows the variation of E, k_T, and α through the cylinder thickness for various values of n.

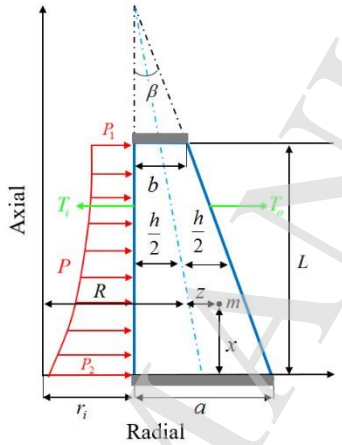

Fig. 1. Axial cross section of the thick cylinder with clamped-clamped ends

It is obvious that in the same position ($-0.5 < z/h < 0.5$), with decreasing n, the dimensionless modulus of elasticity and thermal expansion coefficient decrease but thermal conductivity increases.

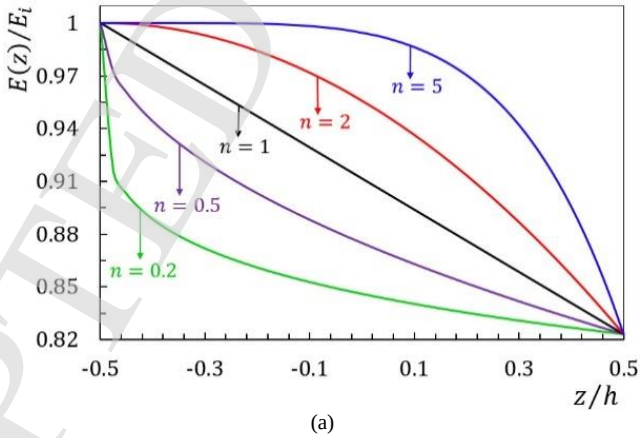

(a)

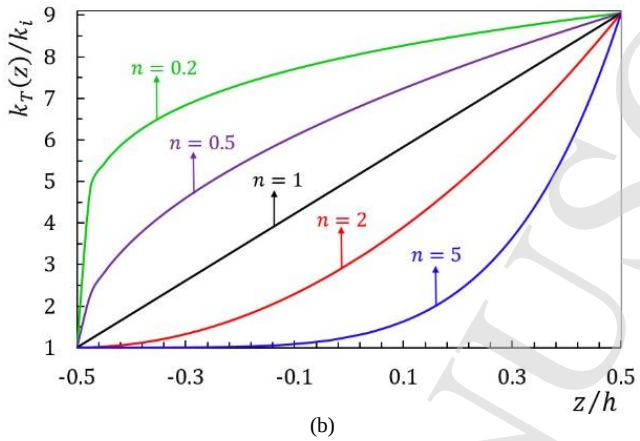

(b)

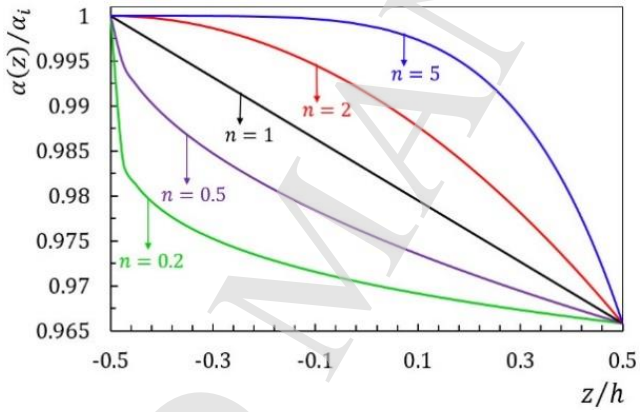

(c)

Fig. 2. Variation of the normalized (a) elasticity module (b) thermal conductivity (c) thermal expansion coefficient along the dimensionless radial direction

2.2. *Thermoelasticity governing equations*

The coordinates of a point on the longitudinal section of the cylinder can be defined by the two parameters *r* and *x*, where *x* is the vertical coordinate, and *r* is the radius, which is perpendicular to *x* and satisfies $r = R + z$ (Fig. 1). Also, R is the middle surface radius, z is the thickness variable, which is changed between $-h/2$ and $+h/2$. R and variable thickness h are:

$$\begin{cases} R = r_i + \dfrac{a}{2} - x\left(\tan\beta/2\right) \\ h = r_i + a - x\left(\tan\beta\right) \end{cases} \tag{2}$$

where β is taper angle as:

$$\beta = tan^{-1}\left(\frac{a-b}{L}\right) \tag{3}$$

FSDT is one of the general theories for thick walled shells. In the FSDT, it is assumed the sections that are perpendicular to mid-plane remain straight after the loading and deformation but are not necessarily perpendicular. Therefore, in FSDT the shear strain and shear stress are considered. According to the FSDT, the displacement of each point of the shell is expressed as the sum of displacement of the middle surface and the displacement of that point respect to the middle surface. The general axisymmetric displacement field (U_x, U_z), in the FSDT could be expressed on the basis of axial and radial displacements, as follow :

$$\begin{Bmatrix} U_x \\ U_z \end{Bmatrix} = \begin{Bmatrix} u(x) \\ w(x) \end{Bmatrix} + z \begin{Bmatrix} \phi(x) \\ \psi(x) \end{Bmatrix} \tag{4}$$

where U_x and U_z denotes the displacement components along the axial, circumferential and radial directions. The displacement components of the middle surface are express by $u(x)$ and $w(x)$. Also, $\phi(x)$ and $\psi(x)$ are unknown functions to determine the displacement field. The kinematic relations in the cylindrical coordinate system are:

$$\begin{cases} \varepsilon_x = \dfrac{\partial U_x}{\partial x} = \dfrac{du(x)}{dx} + \dfrac{d\phi(x)}{dx} z \\ \varepsilon_\theta = \dfrac{U_z}{r} = \dfrac{1}{R+z}\left(w(x) + \psi(x) z\right) \\ \varepsilon_z = \dfrac{\partial U_z}{\partial z} = \psi(x) \\ \gamma_{xz} = \dfrac{\partial U_x}{\partial z} + \dfrac{\partial U_z}{\partial x} = \phi(x) + \left(\dfrac{dw(x)}{dx} + \dfrac{d\psi(x)}{dx} z\right) \end{cases} \tag{5}$$

The thermal stresses on the basis of constitutive equations for isotropic materials are as follow:

$$\begin{cases} \sigma_i = \lambda E\left[(1-v)\left(\varepsilon_i - \varepsilon_i^c\right) + v\left(\left(\varepsilon_j - \varepsilon_j^c\right) + \left(\varepsilon_k - \varepsilon_k^c\right)\right)\right] \\ -\lambda E(1+v)\alpha T \quad , \quad i \neq j \neq k \\ \tau_{xz} = \lambda E\left[(1-2v)\dfrac{\gamma_{xz}}{2}\right] \quad , \quad \lambda = \dfrac{1}{(1+v)(1-2v)} \end{cases} \tag{6}$$

where T is temperature distribution and σ_i, ε_i and ε_i^c are the stresses, strains and creep strains, respectively. Also τ_{xz} and γ_{xz} are the shear stress and shear strain, respectively. The stresses distributed over the thickness of the shell produce normal forces (N_x, N_θ, N_z), bending moments (M_x, M_θ, M_z), shear force (Q_x), and twisting moment (M_{xz}). The moments and forces per unit length are also called stress resultants. The stress resultants are as follow:

$$\begin{cases} \{N_x, N_\theta, N_z\} = \int_{-h/2}^{h/2} \left\{ \sigma_x \left(1+\frac{z}{R}\right), \sigma_\theta, \sigma_z \left(1+\frac{z}{R}\right) \right\} dz \\ \{M_x, M_\theta, M_z\} = \int_{-h/2}^{h/2} \left\{ \sigma_x \left(1+\frac{z}{R}\right), \sigma_\theta, \sigma_z \left(1+\frac{z}{R}\right) \right\} z dz \\ Q_x = K \int_{-h/2}^{h/2} \tau_{xz} \left(1+\frac{z}{R}\right) dz \\ M_{xz} = K \int_{-h/2}^{h/2} \tau_{xz} \left(1+\frac{z}{R}\right) z dz \end{cases} \tag{7}$$

where K is the shear correction factor, which is applied to the shear stress according to the shell geometry. This coefficient is considered $K = 5/6$ in the static state for the cylinder. [Vlachoutsis, 1992]. In order to obtain the equilibrium equations, principle of virtual work is used. According to this, the variations of strain energy are equal to the variations of the virtual work as follows:

$$\delta U = \delta W \tag{8}$$

where in Eq. (8), U and W are the total strain energy and the total virtual work due to internal pressure, respectively. The strain energy is:

$$\begin{cases} U = \iiint_V U^* dV \\ dV = r dr d\theta dx = (R+z)\, dx d\theta dz \\ U^* = \frac{1}{2}\left(\sigma_x \varepsilon_x + \sigma_\theta \varepsilon_\theta + \sigma_z \varepsilon_z + \tau_{xz}\gamma_{xz}\right) \end{cases} \tag{9}$$

The variation of the strain energy is:

$$\delta U = \int_0^{2\pi} \int_0^L \int_{-h/2}^{h/2} \delta U^* (R+z)\, dz dx d\theta \tag{10}$$

The resulting Eq. (10) will be:

$$\frac{\delta U}{2\pi} = \int_0^L \int_{-h/2}^{h/2} \left(\sigma_x \delta\varepsilon_x + \sigma_\theta \delta\varepsilon_\theta + \sigma_z \delta\varepsilon_z + \tau_{xz}\delta\gamma_{xz}\right)(R+z)\, dz dx \tag{11}$$

the virtual work is:

$$\begin{cases} W = \iint_S \left(\vec{f}_{sf}.\vec{u}\right) dS \\ dS = r_i d\theta dx = \left(R - \frac{h}{2}\right) d\theta dx \\ \vec{f}_{sf}.\vec{u} = -PU_z \end{cases} \tag{12}$$

For axial distribution of internal pressure, the model of Eq. (13) is selected as follows:

$$P = P_1 + (P_2 - P_1)\left(\frac{x}{L}\right)^{m_p} \tag{13}$$

Here P_1 and P_2 are the values of pressure at the $x=0$ and $x=L$, respectively. m_p is constant parameter that is used to control the pressure profile. Thus, the variation of the virtual work is:

$$\delta W = \int_0^{2\pi}\int_0^{L}\left(P\delta U_z\right)\left(R-\frac{h}{2}\right)dxd\theta \tag{14}$$

The resulting Eq. (14) will be:

$$\frac{\delta W}{2\pi} = \int_0^{L}\left(P\delta U_z\right)\left(R-\frac{h}{2}\right)dx \tag{15}$$

Substituting Eqs. (11) and (15) into Eq. (8) and drawing upon calculus of variation and the virtual work principle, with regard to Eq. (7), we will have:

$$\begin{cases} \dfrac{d}{dx}\left(RN_x\right)=0 \\ \dfrac{d}{dx}\left(RM_x\right)-RQ_x=0 \\ \dfrac{d}{dx}\left(RQ_x\right)-N_\theta=-P\left(R-\dfrac{h}{2}\right) \\ \dfrac{d}{dx}\left(RM_{xz}\right)-M_\theta-RN_z=P\dfrac{h}{2}\left(R-\dfrac{h}{2}\right) \end{cases} \tag{16}$$

and the boundary conditions at the two ends of the cylinder are:

$$\left[R\left(N_x\delta u+M_x\delta\phi+Q_x\delta w+M_{xz}\delta\psi\right)\right]_0^L=0 \tag{17}$$

Substituting the stress components from Eqs. (6) into Eqs. (7) and then into the equilibrium Eqs. (16), the following set of differential equation for displacement is obtained:

$$\begin{cases} \left[A_1\right]\dfrac{d^2}{dx^2}\{y\}+\left[A_2\right]\dfrac{d}{dx}\{y\}+\left[A_3\right]\{y\}=\{F'\} \\ \{y\}=\left\{u(x) \quad \phi(x) \quad w(x) \quad \psi(x)\right\}^T \end{cases} \tag{18}$$

Eq. (18) is a set of linear non-homogenous equations. $[A_3]$ is irreversible and its reverse is needed in the subsequent calculations. In order to make $[A_3]^{-1}$, the first equation in the set of Eq. (16) is integrated:

$$RN_x = C_0 \tag{19}$$

In Eq. (18), it is apparent that u does not exist, but du/dx does. Taking du/dx as υ:

$$u(x)=\int \upsilon(x)dx + C_7 \tag{20}$$

Thus, set of differential Eq. (18) could be derived as follows:

$$\begin{cases} \left[B_1\right]\dfrac{d^2}{dx^2}\{y\}+\left[B_2\right]\dfrac{d}{dx}\{y\}+\left[B_3\right]\{y\}=\{F\} \\ \{y\}=\left\{\upsilon(x) \quad \phi(x) \quad w(x) \quad \psi(x)\right\}^T \end{cases} \tag{21}$$

where the coefficients matrices $[B_i]_{4\times4}$, and force vector $\{F\}_{4\times1}$ have been defined in the Appendix A.

2.2.1. *Thermoelasticity semi-analytical solution*

The differential Eq. (21) for a variable thickness cylinder is a differential equation with variable coefficients, due to *R* and *h* components that are related to the *x*-axis component, therefore the solution is complex and in some cases impossible. Hence, in the current study, a semi-analytical method based on MLM for the solution of Eq. (21) is presented. In this method, the cylinder is divided into disk layers with constant thickness t_n. Therefore, the MLM is a semi-analytical method and converts the differential equations with variable coefficients into the differential equations with constant coefficients in order to have an analytical solution. [Nejad, Jabbari *et al.*, 2015], (Fig. 3 (a)).

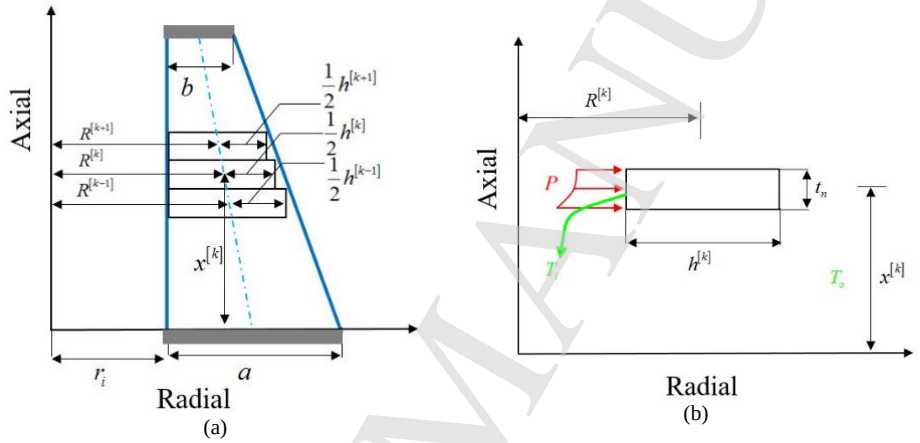

Fig. 3. (a) Division of thick cylinder with variable thickness into homogenous disks with constant thickness (b) Geometry of an arbitrary homogenous disk layer.

Therefore, the governing equations convert to nonhomogeneous set of differential equations with constant coefficients. $x^{[k]}$ and $R^{[k]}$ are length and radius of middle of disks. The length of middle of an arbitrary disk (Fig. 3 (b)) is as follows:

$$x^{[k]} = \left(k - \frac{1}{2}\right)\frac{L}{n_L} \quad , \quad x^{[k]} - \frac{t_n}{2} \le x \le x^{[k]} + \frac{t_n}{2} \quad , \quad t_n = \frac{L}{n_L} \tag{22}$$

where n_L is the number of disks and k is the corresponding number given to each disk. The radius of middle point of each disk is as follows:

$$R^{[k]} = r_i + \frac{h^{[k]}}{2} \quad , \quad h^{[k]} = a - \tan(\beta)x^{[k]} \tag{23}$$

Thus:

$$\frac{dh^{[k]}}{dx} = 2\frac{dR^{[k]}}{dx} = -\tan(\beta) \tag{24}$$

Considering shear stress and based on FSDT, nonhomogeneous set of ordinary differential equations with constant coefficient of each disk is obtained:

$$\begin{cases} \left[B_1\right]^{[k]} \dfrac{d^2}{dx^2}\{y\}^{[k]} + \left[B_2\right]^{[k]} \dfrac{d}{dx}\{y\}^{[k]} + \left[B_3\right]^{[k]}\{y\}^{[k]} = \{F\}^{[k]} \\ \{y\}^{[k]} = \left\{\upsilon(x)^{[k]} \quad \phi(x)^{[k]} \quad w(x)^{[k]} \quad \psi(x)^{[k]}\right\}^T \end{cases} \tag{25}$$

For thermo-elastic analysis of thick cylindrical pressure vessel the creep strains ($\varepsilon_x^c, \varepsilon_\theta^c, \varepsilon_z^c$) are ignored. Defining the differential operator $P(D)$, Eq. (25) is written as:

$$\begin{cases} \left[P(D)\right]^{[k]} = \left[B_1\right]^{[k]} D^2 + \left[B_2\right]^{[k]} D + \left[B_3\right]^{[k]} \\ D^2 = \dfrac{d^2}{dx^2},\ D = \dfrac{d}{dx} \end{cases} \tag{26}$$

Thus

$$[P(D)]^{[k]}\{y\}^{[k]} = \{F\}^{[k]} \tag{27}$$

The differential Eq. (27) has the general solution including homogeneous solution, $\{y\}_h^{[k]}$, and particular solution, $\{y\}_p^{[k]}$. For the homogeneous case:

$$\begin{cases} \left[P(D)\right]^{[k]}\{y\}_h^{[k]} = 0 \\ \{y\}_h^{[k]} = \{V\}e^{m^{[k]}x} \end{cases} \tag{28}$$

Substituting Eq. (28) into Eq. (26):

$$\left|m^2\left[B_1\right]^{[k]} + m\left[B_2\right]^{[k]} + \left[B_3\right]^{[k]}\right| = 0 \tag{29}$$

From the above equation, 6 eigenvalues m_i are determined which are 3 pairs of conjugated root. In order to obtain the eigenvectors $\{V\}_i$, the calculated eigenvalues should be substituted in the following equation:

$$\left[m^2\left[B_1\right]^{[k]} + m\left[B_2\right]^{[k]} + \left[B_3\right]^{[k]}\right]\{V\}^{[k]} = 0 \tag{30}$$

Therefore, the homogeneous solution for Eq. (27) is:

$$\{y\}_h^{[k]} = \sum_{i=1}^{6} C_i^{[k]}\{V\}_i^{[k]} e^{m_i^{[k]}x} \tag{31}$$

The particular solution is obtained as follows:

$$\{y\}_p^{[k]} = \left[B_3^{[k]}\right]^{-1}\{F\}^{[k]} \tag{32}$$

Therefore, the total solution for Eq. (27) is:

$$\{y\}^{[k]} = \sum_{i=1}^{6} C_i^{[k]}\{V\}_i^{[k]} e^{m_i^{[k]}x} + \left[B_3^{[k]}\right]^{-1}\{F\}^{[k]} \tag{33}$$

In general, the problem consists of 8 unknown values of C_i, including C_0 (Eq. (19)), C_1 to C_6 (Eq. (33)), and C_7 (Eq. (20)).

2.2.2. *Boundary and continuity conditions*

The boundary condition of the cylinder is assumed to be clamped-clamped, then

$$\begin{Bmatrix} u(x) \\ \phi(x) \\ w(x) \\ \psi(x) \end{Bmatrix}_{x=0} = \begin{Bmatrix} u(x) \\ \phi(x) \\ w(x) \\ \psi(x) \end{Bmatrix}_{x=L} = \begin{Bmatrix} 0 \\ 0 \\ 0 \\ 0 \end{Bmatrix} \tag{34}$$

Therefore

$$\begin{Bmatrix} U_x(x,z) \\ U_z(x,z) \end{Bmatrix}_{x=0,L} = \begin{Bmatrix} 0 \\ 0 \end{Bmatrix} \tag{35}$$

The main requirement in the disk layer method is that the cylinder is divided into continuous disks. In order to have disk continuity condition, forces, stresses and displacements must be continuous at the boundary between two layers. Hence the continuity conditions are as follows:

$$\begin{Bmatrix} U_x^{[k-1]}(x,z) \\ U_z^{[k-1]}(x,z) \end{Bmatrix}_{x=x^{[k-1]}+t_n/2} = \begin{Bmatrix} U_x^{[k]}(x,z) \\ U_z^{[k]}(x,z) \end{Bmatrix}_{x=x^{[k]}-t_n/2} \tag{36}$$

$$\begin{Bmatrix} U_x^{[k]}(x,z) \\ U_z^{[k]}(x,z) \end{Bmatrix}_{x=x^{[k]}+t_n/2} = \begin{Bmatrix} U_x^{[k+1]}(x,z) \\ U_z^{[k+1]}(x,z) \end{Bmatrix}_{x=x^{[k+1]}-t_n/2} \tag{37}$$

$$\begin{Bmatrix} \frac{dU_x^{[k-1]}(x,z)}{dx} \\ \frac{dU_z^{[k-1]}(x,z)}{dx} \end{Bmatrix}_{x=x^{[k-1]}+t_n/2} = \begin{Bmatrix} \frac{dU_x^{[k]}(x,z)}{dx} \\ \frac{dU_z^{[k]}(x,z)}{dx} \end{Bmatrix}_{x=x^{[k]}-t_n/2} \tag{38}$$

$$\begin{Bmatrix} \frac{dU_x^{[k]}(x,z)}{dx} \\ \frac{dU_z^{[k]}(x,z)}{dx} \end{Bmatrix}_{x=x^{[k]}+t_n/2} = \begin{Bmatrix} \frac{dU_x^{[k+1]}(x,z)}{dx} \\ \frac{dU_z^{[k+1]}(x,z)}{dx} \end{Bmatrix}_{x=x^{[k+1]}-t_n/2} \tag{39}$$

According to continuity conditions, 8 equations are obtained in each disk layer. For a cylinder with n_L disk layers, $8(n_L\text{-}1)$ equations are obtained for the cylinder. Using the 8 equations of the boundary condition, $8n_L$ equations are obtained. The solution of these equations yields $8n_L$ unknown constants.

2.2.3. *Heat conduction analysis*

In the steady-state case and in the absence of heat generation, the heat conduction equation for the one-dimensional problem in polar coordinates simplifies to:

$$\frac{d}{dr}\left[k_T r \frac{dT}{dr}\right] = 0 \tag{40}$$

By considering $r = R + z$, Eq. (40) can be written as follows:

$$\frac{d}{dz}\left[k_T^{[k]}\left(R^{[k]}+z\right)\frac{dT^{[k]}}{dz}\right]=0 \tag{41}$$

Solving the differential Eq. (41) finally the terms of temperature gradient are derived as follows:

$$T^{[k]}=g_1^{[k]}\int_{-h/2}^{z}\frac{dz}{k_T^{[k]}\left(R^{[k]}+z\right)}+g_2^{[k]}-T_{ref} \tag{42}$$

where $g_1^{[k]}$ and $g_2^{[k]}$ are unknown constants which obtained from boundary conditions. In this study, the reference temperature T_{ref} is assumed to be equal to T_o. The temperature boundary conditions is as follow; the internal and external surfaces of the cylinder are expose to T_i and T_o, respectively. By applying boundary conditions, temperature gradient distribution is obtained as Eq. (43). The effect of different values of grading index n, on the non-dimensional temperature change $T/(T_i-T_o)$ along the radial direction is shown in Fig. 4. It can be seen from Fig. 4 that the temperature change along the radial direction in a homogeneous cylinder made of full stainless steel or full zirconia is always greater than that in the FG cylinder.

$$T^{[k]}=T_i\left(1-\frac{\int_{-h^{[k]}/2}^{z}\frac{dz}{k_T^{[k]}\left(R^{[k]}+z\right)}}{\int_{-h^{[k]}/2}^{+h^{[k]}/2}\frac{dz}{k_T^{[k]}\left(R^{[k]}+z\right)}}\right)+T_o\left(\frac{\int_{-h^{[k]}/2}^{z}\frac{dz}{k_T^{[k]}\left(R^{[k]}+z\right)}}{\int_{-h^{[k]}/2}^{+h^{[k]}/2}\frac{dz}{k_T^{[k]}\left(R^{[k]}+z\right)}}\right) \tag{43}$$

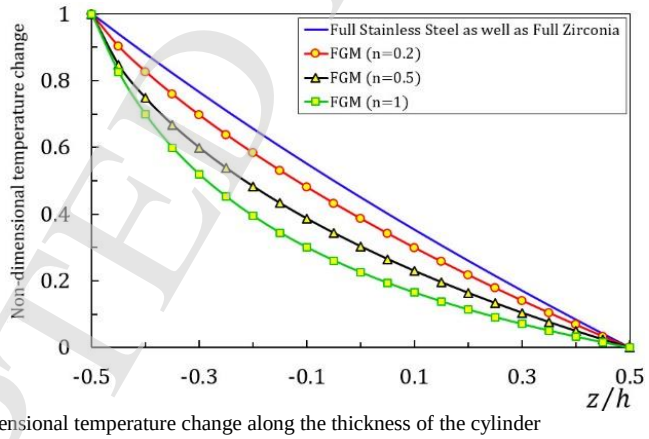

Fig. 4. Non-dimensional temperature change along the thickness of the cylinder

2.3. *Thermoelasticity governing equations for creep*

Using Eqs. (5), the total strain rate–displacement rate relations results:

$$\begin{cases} \dot{\varepsilon}_x = \dfrac{\partial \dot{U}_x}{\partial x} = \dfrac{d\dot{u}(x)}{dx} + \dfrac{d\dot{\phi}(x)}{dx} z \\ \dot{\varepsilon}_\theta = \dfrac{\dot{U}_z}{r} = \dfrac{1}{R+z}\left(\dot{w}(x) + \dot{\psi}(x) z\right) \\ \dot{\varepsilon}_z = \dfrac{\partial \dot{U}_z}{\partial z} = \dot{\psi}(x) \\ \dot{\gamma}_{xz} = \dfrac{\partial \dot{U}_x}{\partial z} + \dfrac{\partial \dot{U}_z}{\partial x} = \dot{\phi}(x) + \left(\dfrac{d\dot{w}(x)}{dx} + \dfrac{d\dot{\psi}(x)}{dx} z \right) \end{cases} \tag{44}$$

where:

$$\dot{(\ )} = \frac{d(\ )}{dt} \tag{45}$$

For isotropic cylinder with creep behavior, the relations between rates of stress and strain are:

$$\begin{cases} \dot{\sigma}_i = \lambda E\left[(1-v)\left(\dot{\varepsilon}_i - \dot{\varepsilon}_i^c\right) + v\left(\left(\dot{\varepsilon}_j - \dot{\varepsilon}_j^c\right) + \left(\dot{\varepsilon}_k - \dot{\varepsilon}_k^c\right)\right)\right] \quad , \quad i \neq j \neq k \\ \dot{\tau}_{xz} = \lambda E\left[(1-2v)\dfrac{\dot{\gamma}_{xz}}{2} \right] \end{cases} \tag{46}$$

where $\dot{\sigma}_i$, $\dot{\varepsilon}_i$ and $\dot{\varepsilon}_i^c$ are stresses, strains and the creep strains rate, respectively. In addition, $\dot{\tau}_{xz}$ and $\dot{\gamma}_{xz}$ are the shear stress and shear strain rate, respectively. Using Norton's law:

$$\begin{cases} \dot{\varepsilon}_i^c = \dfrac{A\sigma_e^{(n_c-1)}}{2}\left[2\sigma_i - \left(\sigma_j + \sigma_k\right)\right] \quad , \quad i \neq j \neq k \\ \sigma_e = \dfrac{1}{\sqrt{2}}\sqrt{\left(\sigma_x - \sigma_\theta\right)^2 + \left(\sigma_x - \sigma_z\right)^2 + \left(\sigma_z - \sigma_\theta\right)^2 + 6{\tau_{xz}}^2} \end{cases} \tag{47}$$

where A and n_c are material constants for creep. Using Eqs. (16) and considering the pressure to be constant with time, the equilibrium equation for creep analysis is:

$$\begin{cases} \dfrac{d}{dx}\left(R\dot{N}_x\right) = 0 \\ \dfrac{d}{dx}\left(R\dot{Q}_x\right) - \dot{N}_\theta = 0 \\ \dfrac{d}{dx}\left(R\dot{M}_x\right) - R\dot{Q}_x = 0 \\ \dfrac{d}{dx}\left(R\dot{M}_{xz}\right) - \dot{M}_\theta - R\dot{N}_z = 0 \end{cases} \tag{48}$$

Considering the temperature field to be steady, the following set of differential equations for displacement rates is obtained as follows:

$$\begin{cases} [B_1]\dfrac{d^2}{dx^2}\{\dot{y}\}+[B_2]\dfrac{d}{dx}\{\dot{y}\}+[B_3]\{\dot{y}\}=\{F_c\} \\ \{\dot{y}\}=\left\{\dot{\upsilon}(x) \quad \dot{\phi}(x) \quad \dot{w}(x) \quad \dot{\psi}(x)\right\}^T \end{cases} \tag{49}$$

where the force vector $\{F_c\}_{4\times1}$ has been defined in the Appendix B. Using the same approach to solve the set of non-homogenous linear differential Eq. (21), the solution for the Eq. (49) can be written in the form of:

$$\{\dot{y}\}^{[k]}=\sum_{i=1}^{6}D_i^{[k]}\{V\}_i^{[k]}e^{m_i^{[k]}x}+\left[B_3^{[k]}\right]^{-1}\{F_c\}^{[k]} \tag{50}$$

where D_i are unknown values. When the stresses rate is known, the calculation of stresses at any time t_i should be performed iteratively:

$$\begin{cases} \sigma_{ij}^{(i)}(r,t_i)=\sigma_{ij}^{(i-1)}(r,t_{i-1})+\dot{\sigma}_{ij}^{(i)}(r,t_i)\,dt^{(i)} \\ t_i=\sum_{k=0}^{i}dt^{(k)} \end{cases} \tag{51}$$

The solution of $t_i=0$ corresponds to that for thermo-elastic material behavior. To calculate $\dot{\sigma}_{ij}^{(i)}(r,t_i)$, the stresses at the time t_{i-1} used.

3. Validation and numerical results

In the previous section, the analytical solution of creep stresses for an FG thick cylindrical pressure vessel with variable thickness subjected to a temperature gradient and non-uniform internal pressure based on the FSDT and MLM, was obtained. This section, presents some numerical case studies for verifying the accuracy of the present theory in predicting the creep stress responses of thick FG cylinder. The geometrical characteristics of the cylinder are assumed as $r_i=40$ mm, $a=20$ mm, $b=10$ mm and $L=800$ mm. The FG cylinder is taken to be made of stainless steel and zirconia with the following material properties (Table 1):

Table 1. Stainless steel and zirconia material properties [Kordkheili and Livani, 2013]

Zirconia	$E_i=244.27$ GPa	$k_i=1.7$ W/m°C	$\alpha_i=12.76\times10^{-6}$ 1/°C	$\nu=0.32$
Stainless steel	$E_o=201.04$ GPa	$k_o=15.38$ W/m°C	$\alpha_o=12.33\times10^{-6}$ 1/°C	$\nu=0.32$

It must be noted that the same grading index (n) has been used in this study while defining the material properties for the modulus of elasticity, the thermal conductivity and the thermal expansion coefficient. The internal pressure applied at the $x=0$ and $x=L$ is $P_1=120$ MPa and $P_2=40$ MPa, respectively. The FG thick cylinder has clamped-clamped boundary conditions. The boundary conditions for temperature are taken as $T_i=800$ °C and $T_o=785$ °C. The creep constants for steady state creep status are considered as

$A = 5.2 \times 10^{-56}$, $n_c = 5.4$ [Kordkheili and Livani, 2013]. The results are presented in a non-dimensional form. Displacements are normalized by dividing to the internal radius. In this study, the mean internal pressure parameter were defined as follows in order to normalize stresses:

$$\bar{P} = \left(P_1 + P_2\right)/2$$

In order to show the effectiveness and accuracy of the approach suggested here, a comparison between responses of the present theory and FEM can be made. In FEM, a thick FG cylinder was modeled using ANSYS®. The PLANE 223 element in axisymmetric mode, which is an element with eight nodes with up to four degrees of freedom per each node, was used for discretization. In order to model FG cylinder, an innovative application for multi-layering of thickness in the radial direction has been performed. Homogenous layers which are of identical thickness and step-variable elasticity modulus have been formed by this method. The cylinder with variable thickness consists of some coherent homogeneous layers whose properties at the contact location of the layers are the average o left and right limit of two layers boundaries. Internal non-uniform pressure are applied to the nodes of inner layers. Fig. 5 illustrates a valid range for using number of FG layers in calculating the radial displacement after 1000 hr of creeping in middle layer. It could be observed that if the number of FG layers is more than 20 layers, there will be no significant effect on radial displacement. In this paper, the cylinder along the radial direction divided to 20 equal and joined layers by the assumption of inhomogeneity constant equal to $n = 1$ .Fig. 6 illustrates the finite-element model is established with ANSYS®. There is a good agreement among numerical results based on FSDT and FEM.

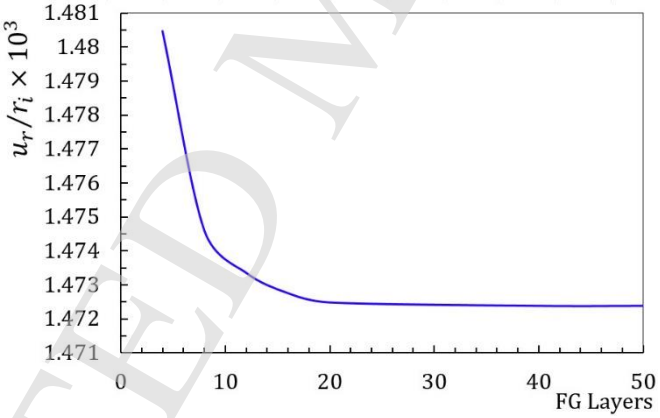

Fig. 5. Effect of the number of FG layers on the radial displacement after 1000 hr of creeping in middle layer ($x = L/2$, $n = 1$, $m_p = 1$)

(a)

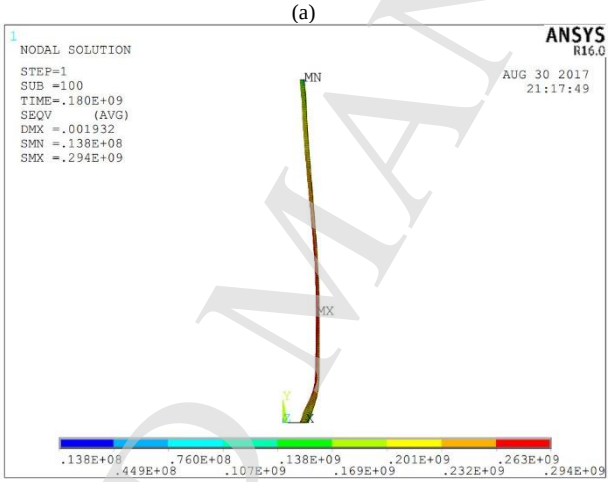

(b)

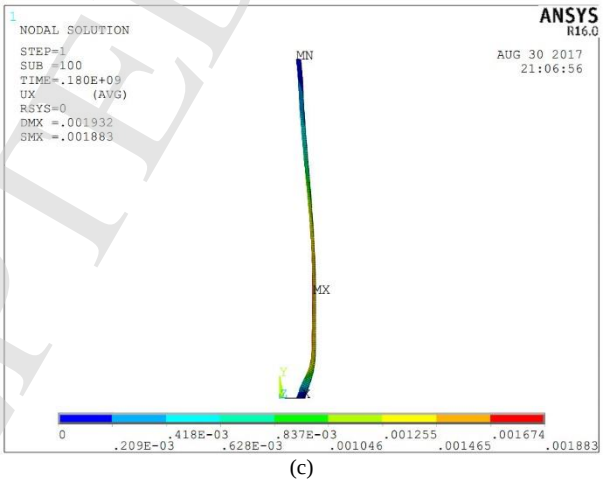

(c)

Fig. 6. Finite-element model for the cylinder with variable thickness (a) FG Layers (b) Von Mises stress in the cylinder (c) Radial displacement distribution in the cylinder after 50000 hr of creeping ($n = 1$, $m_p = 1$)

Table 2 presents the results of the different solutions for the thick cylinder under mechanical and thermal loading at the middle layer of the cylinder ($x = L/2$) and middle layer ($z = 0$), from initial thermo-elastic (initial solution) distribution to final distribution at the fourth selected time step in hour (hr). Relevant results have also been obtained for the creep displacements and stresses curves through the axial direction of the cylinder in Figs. 7 and 8, which verify the results obtained in Table 2.

Table 2. Numerical results based on FSDT and FEM at different creep times

		Initial solution	$t = 1000\ hr$	$t = 10000\ hr$	$t = 30000\ hr$	$t = 50000\ hr$
$\frac{u_r}{r_i} \times 1000$	FSDT	1.1700	1.4730	3.2952	7.2028	11.1081
	FEM	1.1753	1.4355	3.2647	7.1750	11.0823
$\frac{u_x}{r_i} \times 1000$	FSDT	-0.2772	-0.6468	-2.6520	-5.7985	-8.8170
	FEM	-0.4952	-0.8957	-2.8700	-6.0165	-9.0350
$\frac{\sigma_r}{\overline{P}}$	FSDT	-0.4059	-0.4306	-0.4527	-0.4535	-0.4535
	FEM	-0.3859	-0.4229	-0.4451	-0.4456	-0.4456
$\frac{\sigma_\theta}{\overline{P}}$	FSDT	2.6336	2.7423	2.6721	2.6547	2.6542
	FEM	2.6851	2.7435	2.6805	2.6783	2.6781
$\frac{\sigma_x}{\overline{P}}$	FSDT	0.4871	0.6121	0.9868	1.0831	1.0885
	FEM	0.5503	0.6745	1.0500	1.1463	1.1518
$\frac{\tau_{rx}}{\overline{P}}$	FSDT	-0.0585	-0.0628	-0.0542	-0.0637	-0.0636
	FEM	-0.00459	-0.00885	-0.00023	-0.00971	-0.00970
$\frac{\sigma_e}{\overline{P}}$	FSDT	2.7077	2.8032	2.7106	2.6941	2.6936
	FEM	2.7262	2.7848	2.7077	2.7055	2.7055

In Figs. 7 and 8, creep displacement and stress distributions at different layers obtained, using FSDT, are compared with the solutions of FEM and are presented in the form of graphs for $n = 1$. The radial displacement at points away from the boundary regions depends on radius and length. According to Fig. 7, the greatest axial and radial displacement occurs in the internal surface ($z = -h/2$). It is obviously apparent from Figs. 7 and 8 that creep displacements and stresses at points near the boundaries, are different from the other areas under the effect of shear stresses resulted from clamped boundary condition. At points away from the boundaries, displacements and stresses does not show significant variations along the longitudinal direction, while at points near the boundaries, the reverse holds true. Figs. 7 and 8 show that the FSDT has an acceptable amount of accuracy when one wants to obtain creep displacements and stresses.

For the verification of the analytical solution in this paper, plots of the normalized radial and circumferential stress distributions using the presented FSDT and the analytical solution (Nejad & kashkoli, 2014) along the dimensionless radial direction after 10 hr of creeping are given in Fig. 9. Fig. 9 is obtained for a cylindrical pressure vessel with constant thickness under thermal and mechanical loadings. According to Fig. 9 the results are comparable for this case and good agreement was found.

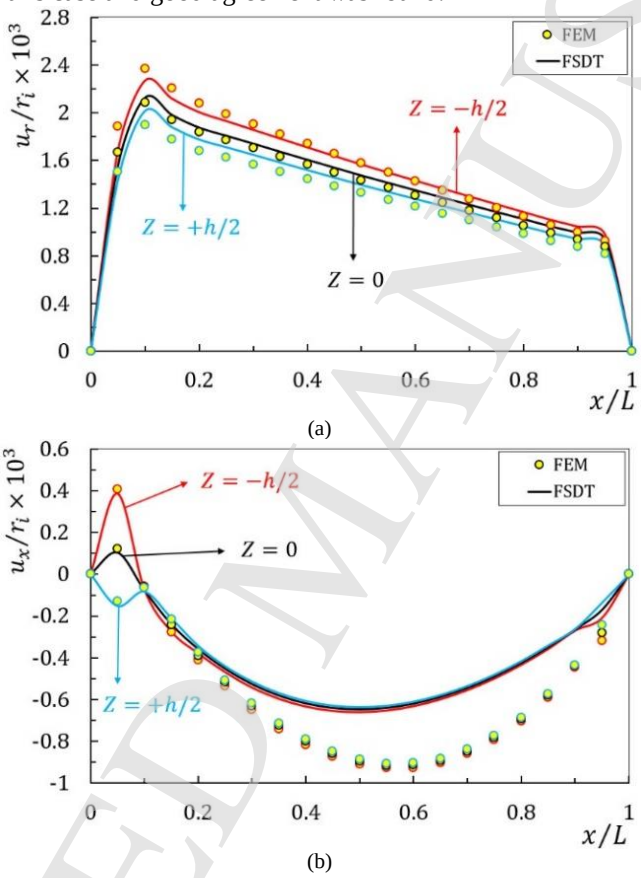

Fig. 7. Variation of normalized radial and axial displacement along the dimensionless axial direction after 1000 hr of creeping at different layers ($n = 1$, $m_p = 1$)

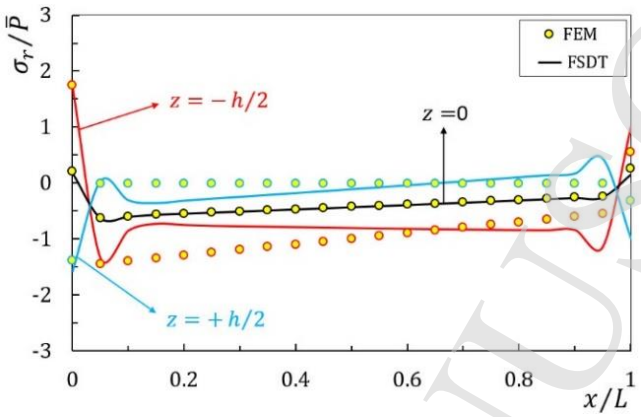

(a)

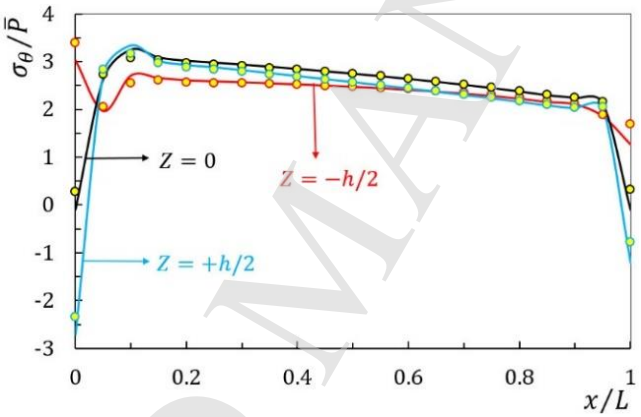

(b)

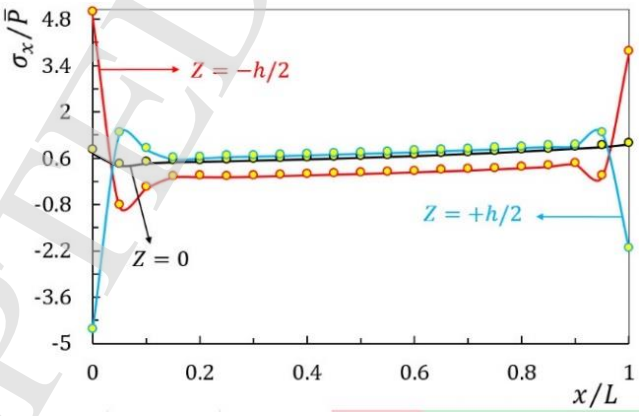

(c)

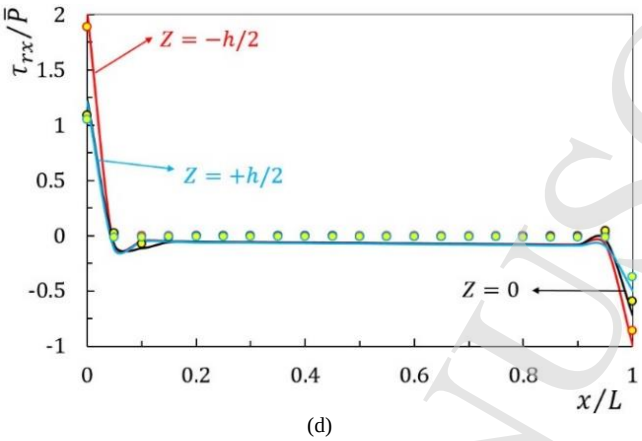

(d)

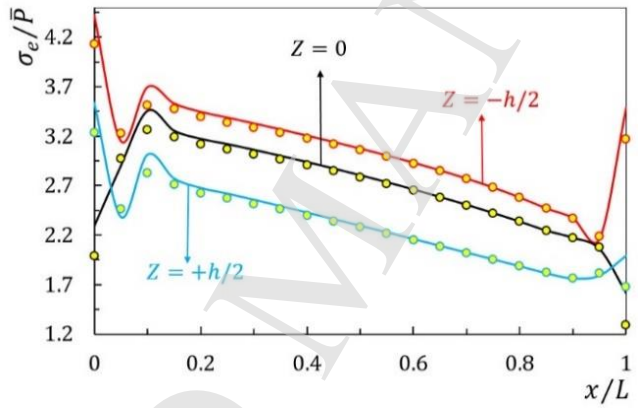

(e)

Fig. 8. Variation of normalized stresses along the dimensionless axial direction after 1000 hr of creeping at different layers ($n = 1$, $m_p = 1$)

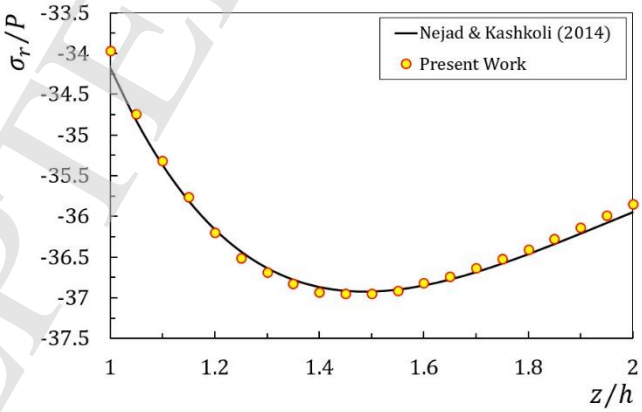

(a)

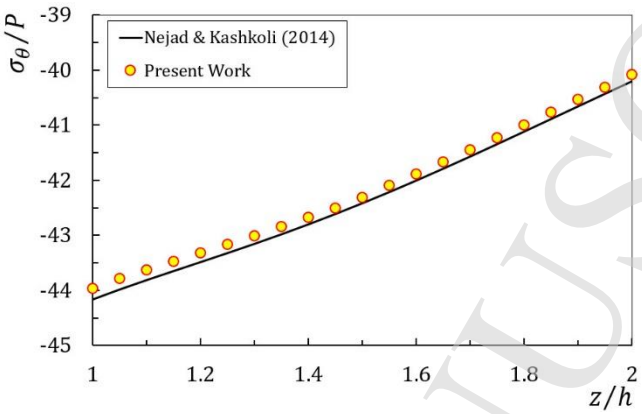

(b)

Fig. 9. Variation of normalized radial and circumferential stresses along the dimensionless radial direction after 10 hr of creeping ($n = 0.3$, $P = 80\ MPa$)

Comparison between the results obtained from FSDT and FEM indicates that the analytical solution based on FSDT has an acceptable amount of accuracy when one wants to obtain radial, circumferential, axial and shear stresses and radial displacement, but it is not that useful for axial displacement. The higher-order approximations are more important for the axial displacement in the FG cylindrical shell with variable thickness. Do to the fact that there has been no solution on creep response of FG cylindrical shell with variable thickness based on HSDT, therefore the result of axial displacement distribution based on FSDT and HSDT are validated with the analytical solution (Jabbari et al., 2015) in an axially functionally graded rotating thick cylindrical shell with variable thickness. It can be seen from Fig. 10 that HSDT must be applied in order to improve the accuracy of the theory.

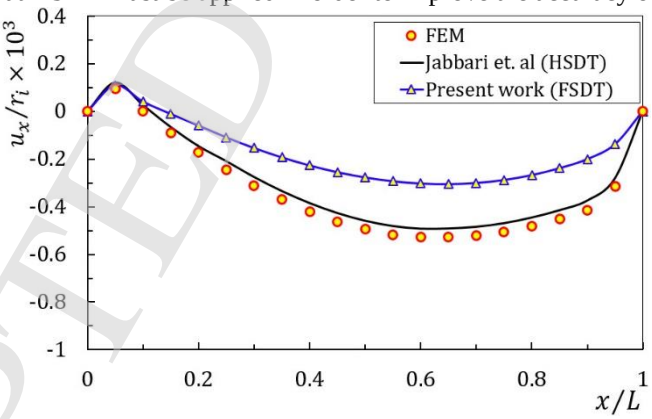

Fig. 10. Variation of normalized axial displacement along the dimensionless axial direction for initial solution (thermo-elastic) in middle layer for different theories ($n = 1$, $m_p = 1$)

The responses of an FG cylinder under mechanical and thermal loads can be considered in order to evaluate the effect of non-homogeneity of used materials. For this purpose, the influences of gradient index on the distribution of creep displacements and stresses along

middle surface are examined in Fig. 11. It could be observed that the absolute values of radial and axial displacement decreases with increase in the grading index n. Another remarkable point to be made from Fig. 11 is that changes in the gradient index have less dramatic effects on the effective stress, as compared with those in the displacements.
Fig. 12 shows the distribution of the normalized displacements and effective stress at the middle of the cylinder after 1000 hr of creeping for various gradient index. It is obvious that with increasing n, the absolute values of radial and axial displacement decrease. It must be noted that for all values of gradient index, the maximum effective stress occur at the inner surface of the cylinder and the minimum at the outer surface.
Histories of normalized displacements and stresses from initial solution at zero time up to 50000 hr for material identified by $n=1$ in middle layer are shown in Figs. 13 and 14, respectively. It is clear from these figures that the absolute values of radial and axial displacements and axial stress increases with time, during creep process of the FG cylinder. It must be noted that the maximum values of radial displacement occur at $x/L=0.1$ for all creep times. Also, Fig. 14 shows that minimum changes will occur for radial, circumferential and effective stresses with time during creep process.

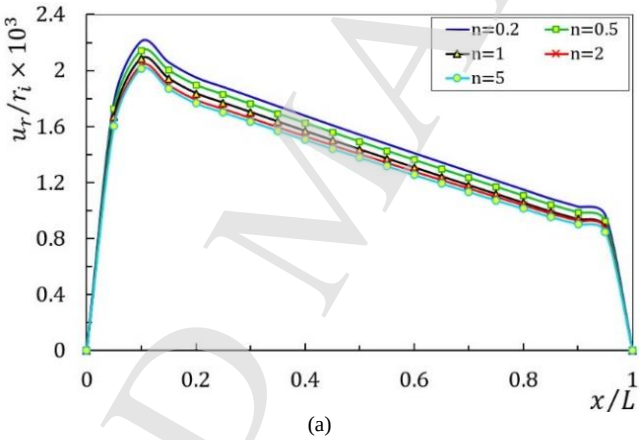

(a)

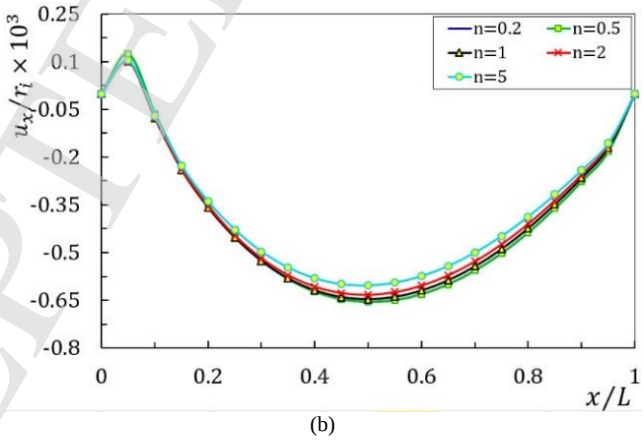

(b)

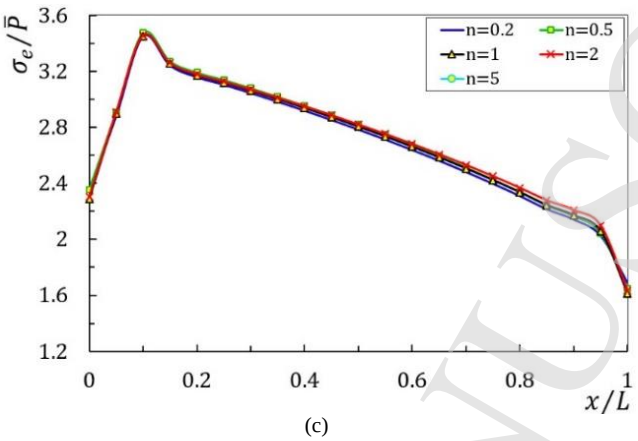

(c)

Fig. 11. The effect of gradient index on the normalized (a) radial displacement (b) axial displacement (c) effective stress along the dimensionless axial direction after 1000 hr of creeping in middle layer ($m_p = 1$)

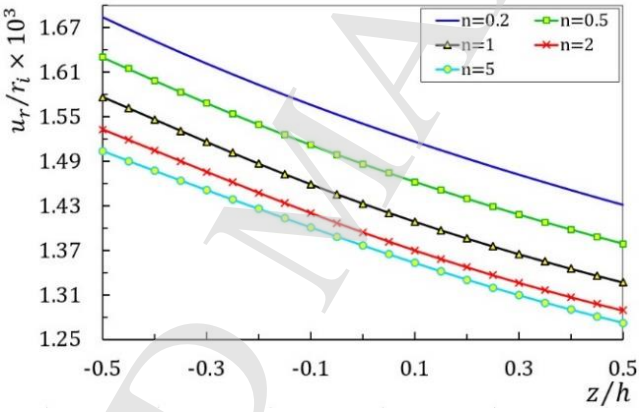

(a)

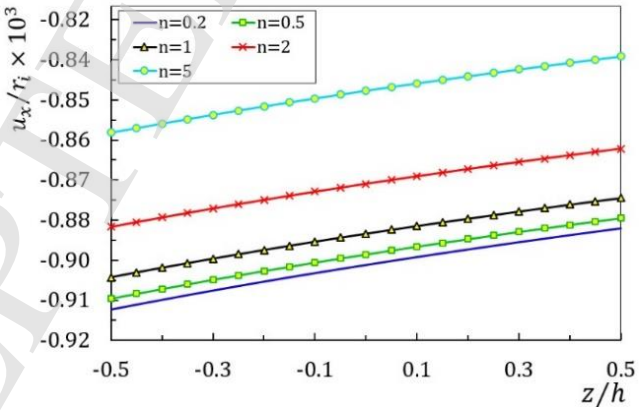

(b)

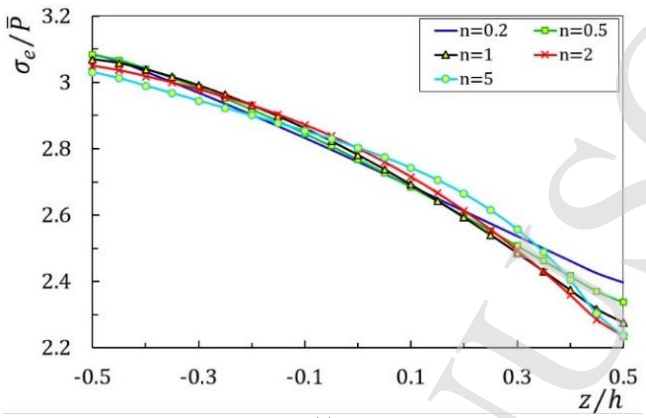

(c)

Fig. 12. The effect of gradient index on the normalized (a) radial displacement (b) axial displacement (c) effecti stress along the dimensionless radial direction after 1000 hr of creeping at $x = L/2$ ($m_p = 1$)

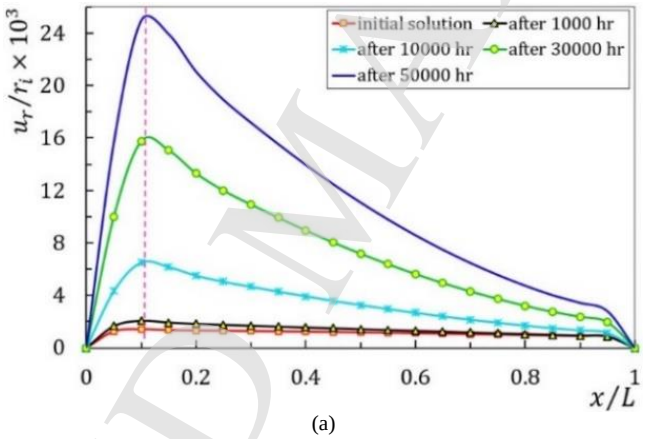

(a)

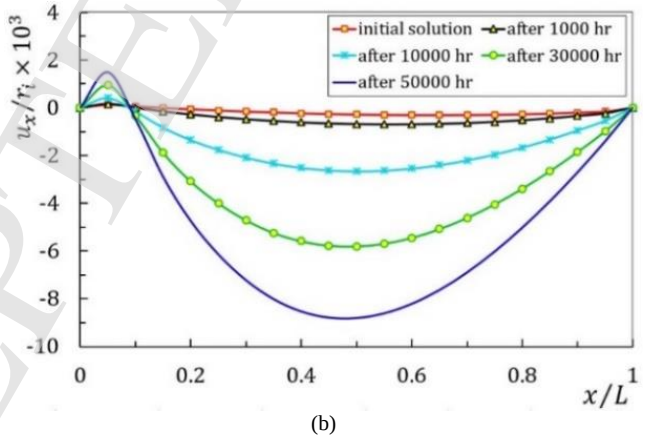

(b)

Fig. 13. Variation of normalized radial and axial displacement along the dimensionless axial direction from initial solution at zero time up to 50000 hr ($n = 1$, $m_p = 1$)

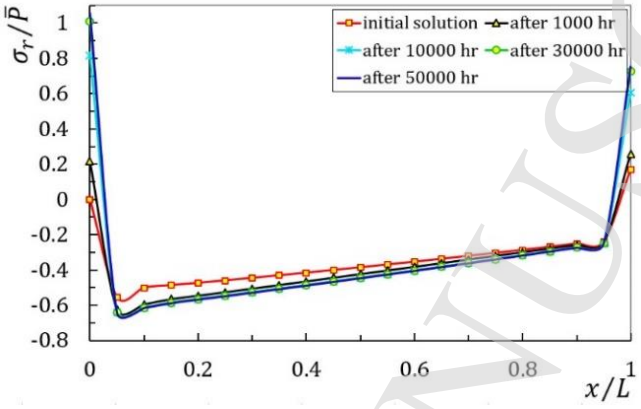

(a)

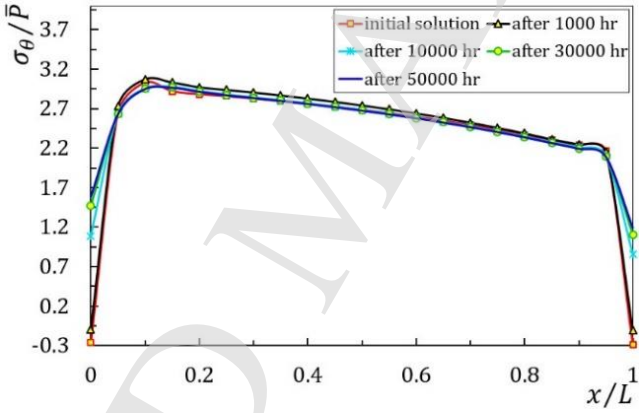

(b)

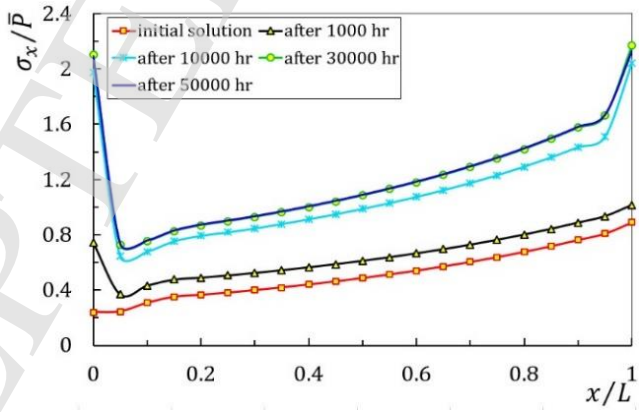

(c)

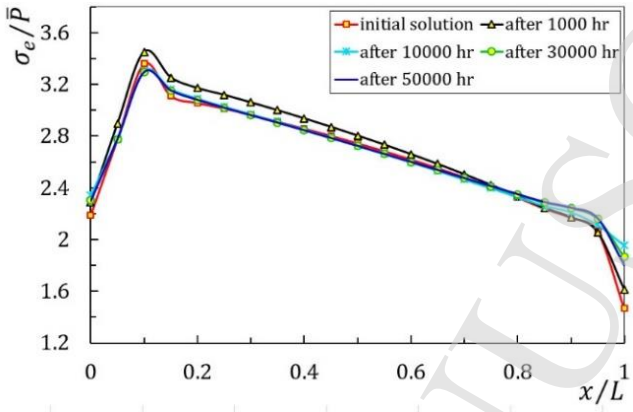

(d)

Fig. 14. Variation of normalized stresses along the dimensionless axial direction from initial solution at zero time up to 50000 hr ($n = 1$, $m_p = 1$)

The effect of the non-uniformity pressure function parameter m_p on the creep response of cylinder is shown in Fig. 15. Fig. 15(a) shows the distribution of pressure function along the dimensionless axial direction. According to Fig. 15(a), the maximum internal pressure occur for $m_p = 2$. It can be seen from Figs. 15 (b) and (d) that, with increasing non-uniformity pressure constant m_p, radial displacement and effective stress increase. It can be observed from Fig. 15(c) that axial displacement distribution does not change with respect to the internal pressure profile. Another remarkable point to be made from Fig. 15(c) is that the distribution of axial displacement for $m_p = 0$ is positive.

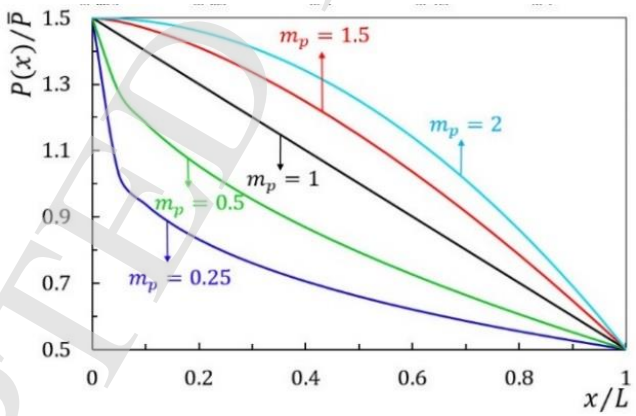

(a)

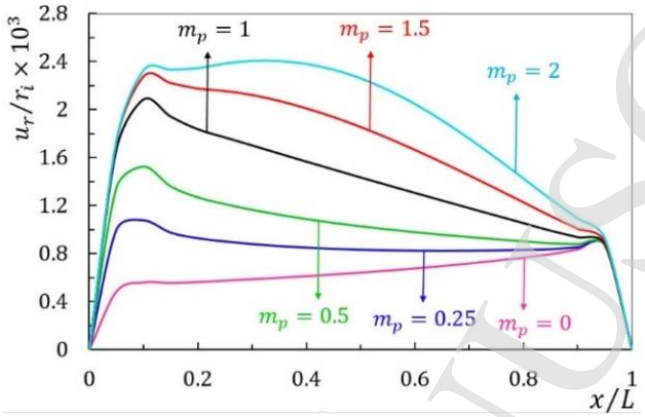

(b)

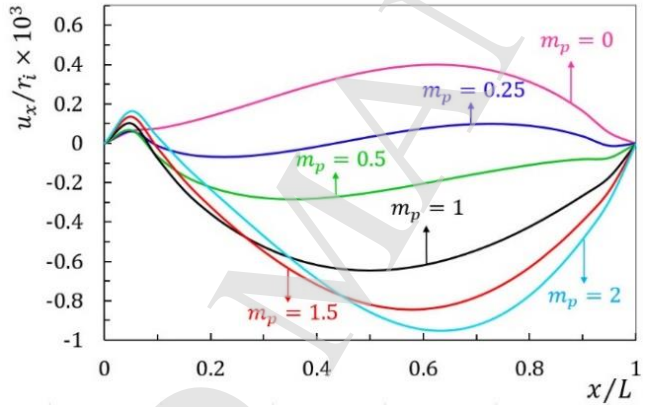

(c)

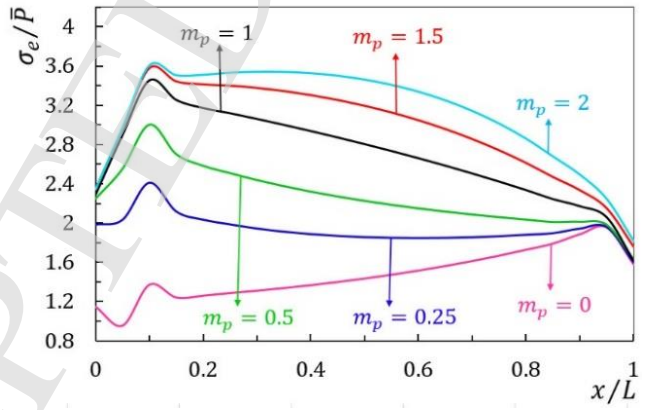

(d)

Fig. 15. The effect of the non-uniformity pressure constant on the normalized (a) pressure profile (b) radial displacement (c) axial displacement (d) effective stress along the dimensionless axial direction after 1000 hr of creeping in middle layer ($n = 1$)

Fig. 16 clearly reflects the influence of the different values of the thermal gradient in the dimensionless displacements and effective stress resultant in middle layer of the thick cylinder. Fig. 16 (a) and (b) show that for $\Delta T \le 0$, with increasing ΔT, absolute values of radial displacement increases but axial displacement decreases, also for $\Delta T > 0$, with increasing ΔT, absolute values of radial displacement decreases but axial displacement increases. It is obvious from Figs. 16 (c) and (d) that for $\Delta T \le 0$ and $\Delta T > 0$, with increasing ΔT effective stress increase. It is evident that the temperature boundary condition is one of the key elements need to be carefully considered when analyzing the working responses of FG cylinders.

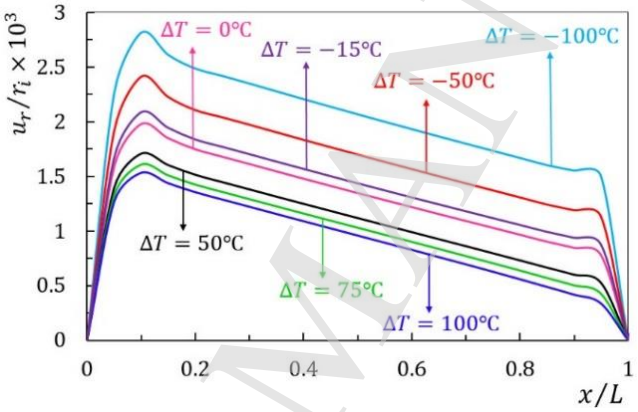

(a)

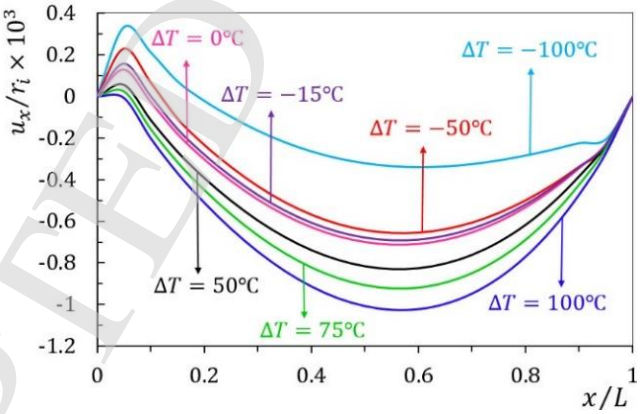

(b)

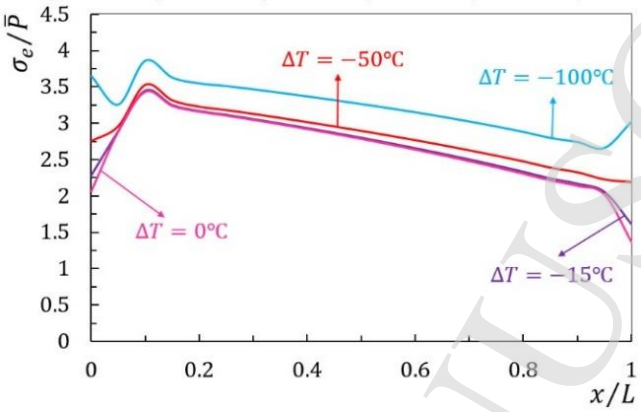

(c)

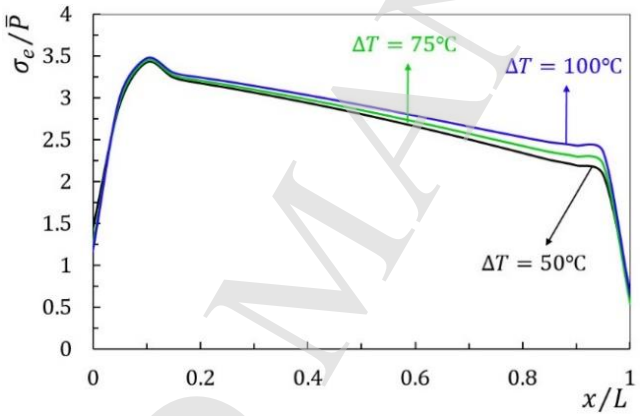

(d)

Fig. 16. The effect of the thermal gradient on the normalized (a) radial displacement (b) axial displacement (c) effective stress ($\Delta T \le 0$) (d) effective stress ($\Delta T > 0$) along the dimensionless axial direction after 1000 hr of creeping in middle layer ($n = 1$, $m_p = 1$)

Fig. 17 illustrates the creep radial and axial displacements and effective stress distributions change with respect to various loading conditions. It has been found that the absolute minimum values of displacements and effective stress distribution belongs to thermal loading. Adding mechanical load will increase displacements and effective stress distribution.

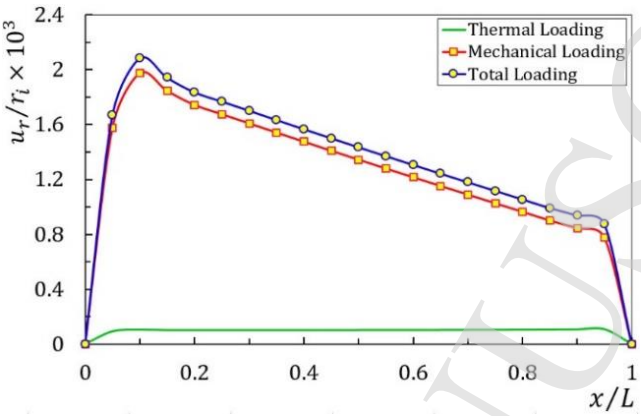

(a)

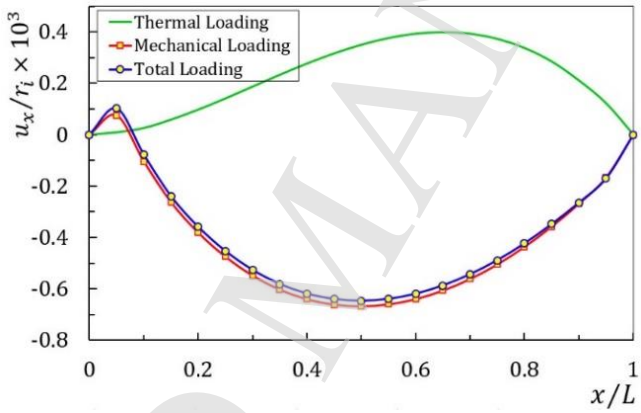

(b)

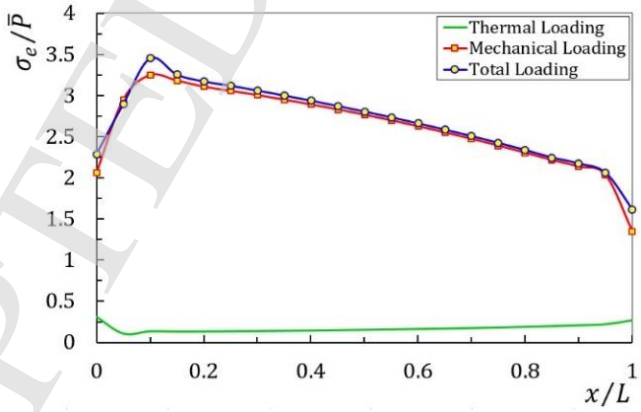

(c)

Fig. 17. The effect of the thermal and mechanical loading on the normalized (a) radial displacement (b) axial displacement (c) effective stress along the dimensionless axial direction after 1000 hr of creeping in middle layer ($n=1$, $m_p=1$)

Histories of radial, circumferential and axial creep strains are plotted in Fig. 18. Creep strains satisfy the incompressibility condition ($\varepsilon_r^c+\varepsilon_\theta^c+\varepsilon_x^c=0$ or $\dot{\varepsilon}_r^c+\dot{\varepsilon}_\theta^c+\dot{\varepsilon}_x^c=0$). The absolute value of both radial and axial creep strains with time is much higher at the internal surface as compared with the external, but the circumferential creep strain is inversed. As far as, the rate of change is concerned, this seems to increases to a maximum between 10000 and 30000 hours, and then decreases until it reaches steady state around 70000 hours of operation.

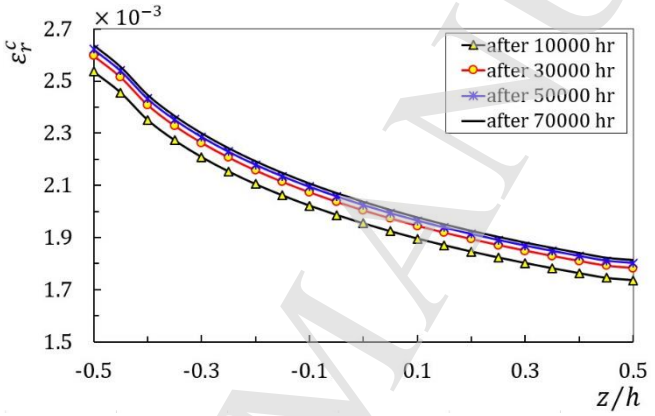

(a)

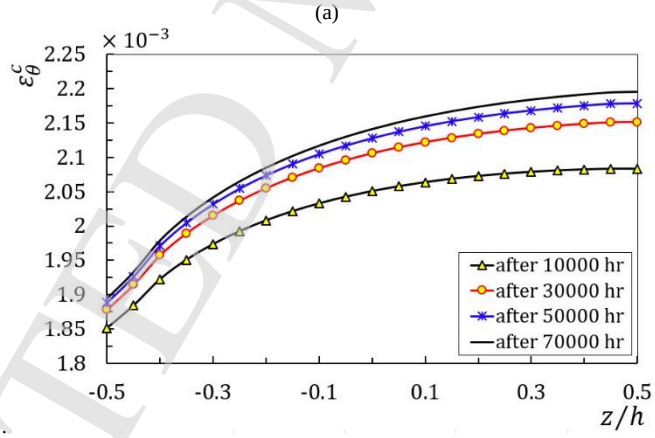

(b)

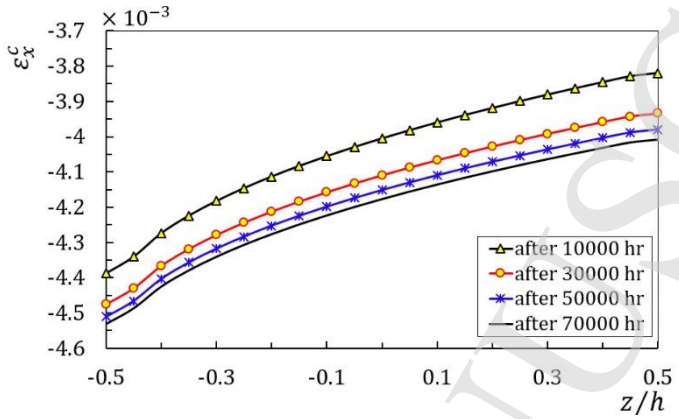

(c)

Fig. 18. Variation of radial, circumferential and axial creep strains along the dimensionless radial direction up to 70000 hr ($n = 1$, $m_p = 1$)

4. Conclusion

In this study, making use of FSDT and MLM, an analytical solution was presented for the purpose of creep analysis of an FGM thick-walled cylinder with variable thickness subjected a temperature gradient and non-uniform internal pressure. The mechanical and thermal properties except Poisson ratio, are graded along the radial direction according to a power law form of radial direction. Finite element analysis of the problem, using ANSYS® was used for the verification purposes of the analytical solution. Good agreement was found between the results. The summary of the conclusions of this study is as follows:

- FGM thick-walled cylindrical shells could be solved using the analytical and semi-analytical methods (e.g. series, perturbation theory). First order shear deformation theory and perturbation theory result in the analytical solution of the problem with higher accuracy and within a shorter period of time. However, the above-mentioned solutions are complicated and time-consuming. The multi-layer method could be a good replacement for the analysis of thick-walled shells. In this method, shells with different geometries and different loadings and different boundary conditions, with even variable pressure, could be more easily solved. This method can be used successfully for nonlinear assumptions (such as creep problem) as well as linear ones.
- The effect of shear deformations in the cylinder especially at the clamped boundaries could be predicted by FSDT. These shear deformations tend to significant gradient of displacement and consequently significant shear stress.
- It can be concluded that existence of shear stresses causes abrupt changing the displacement at the near of two ends of the cylinder (clamped boundaries), therefore, the value of stresses at the two ends of the cylinder are very greater than the stresses at the middle of the cylinder, while zero values of shear stresses at the points far away from the clamped ends causes the corresponding stresses to be constant through the axial direction. These stresses cause stress concentration in the cylinder boundary regions and FSDT help to calculate the stress concentration factor due to end supports.
-

- At very near the axial boundaries of the cylinder, the thermal stresses show a characteristic different from its general behavior over the maximum part of the cylinder. In this very small region, due to edge moments, the absolute values of thermal stresses have a higher value from the points away from boundaries. Also, due to the fact that the two ends of the cylinder is clamped, in the clamped location, the adjacent layer is without moving, While a subsequent layer is capable of moving, this sudden change causes a significant increase in displacements and so a significant increase in stresses. While at the region away from the boundaries, due to the very slight movement of the layers relative to each other, stresses variations are low.
- In the concurrent presence of temperature gradient and non-uniform pressure, achieved results show that the absolute values of radial and axial displacements of the cylinder decrease with increasing the gradient index (n) in both axial and radial directions.
- The superposition law is satisfied for the thermo-elastic creep analysis of FG cylinder with variable thickness.
- Due to the considerable effects of the temperature gradient on the creep response of the cylinder, so the temperature boundary condition is so important and need to be carefully considered.
- Significant changes will occur for radial and axial displacements and axial stress with time during creep process.
- Comparison between the results obtained from FSDT and FEM indicates that the analytical solution based on FSDT has an acceptable amount of accuracy when one wants to obtain radial, circumferential, axial and shear stresses and radial displacement.
- Due to the fact that the volume change due to creep is zero, the volumetric creep strain is zero, and the creep strains satisfy the incompressibility condition. According to the history of creep strains and stresses, creep behavior of these is fairly similar as changes in the rates for these become less significant after 10000 hr, begin to converge after 30000 hr, and reaches steady state after 70000 hr of operation.

Appendix A

$$[B_1]=\begin{bmatrix} 0 & 0 & 0 & 0 \\ 0 & (1-\nu)RX_2 & 0 & 0 \\ 0 & 0 & \frac{(1-2\nu)}{2}RX_0 & \frac{(1-2\nu)}{2}RX_1 \\ 0 & 0 & \frac{(1-2\nu)}{2}RX_1 & \frac{(1-2\nu)}{2}RX_2 \end{bmatrix} \tag{A.1}$$

$$[B_2]=\begin{bmatrix} 0 & (1-\nu)RX_1 & 0 & 0 \\ (1-\nu)RX_1 & (1-\nu)\frac{d}{dx}(RX_1) & \frac{(2\nu-1)}{2}RX_0+\nu\Upsilon_1 & \frac{(4\nu-1)}{2}RX_1+\nu\Upsilon_2 \\ 0 & -\frac{(2\nu-1)}{2}RX_0-\nu\Upsilon_1 & \frac{(1-2\nu)}{2}\frac{d}{dx}(RX_0) & \frac{(1-2\nu)}{2}\frac{d}{dx}(RX_1) \\ 0 & -\frac{(4\nu-1)}{2}RX_1-\nu\Upsilon_2 & \frac{(1-2\nu)}{2}\frac{d}{dx}(RX_1) & \frac{(1-2\nu)}{2}\frac{d}{dx}(RX_2) \end{bmatrix} \tag{A.2}$$

$$[B_3]=\begin{bmatrix} (1-\nu)RX_0 & 0 & \nu\Upsilon_0 & \nu(RX_0+\Upsilon_1) \\ (1-\nu)\frac{d}{dx}(RX_1) & -\frac{(1-2\nu)}{2}RX_0 & \nu\frac{d}{dx}\Upsilon_1 & \nu\frac{d}{dx}(RX_1+\Upsilon_2) \\ -\nu\Upsilon_0 & \frac{(1-2\nu)}{2}\frac{d}{dx}(RX_0) & -(1-\nu)Z_0 & -(1-\nu)Z_1-\nu\Upsilon_0 \\ -\nu(RX_0+\Upsilon_1) & \frac{(1-2\nu)}{2}\frac{d}{dx}(RX_1) & -(1-\nu)Z_1-\nu\Upsilon_0 & -(1-\nu)(Z_2+RX_0)-2\nu\Upsilon_1 \end{bmatrix} \tag{A.3}$$

$$\{F\}=\begin{Bmatrix} C_0+R\Lambda_{1,0} \\ (1+\nu)\frac{d}{dx}(R\Lambda_{1,1}) \\ -P\left(R-\frac{h}{2}\right)-I_{0,0} \\ P\frac{h}{2}\left(R-\frac{h}{2}\right)-(I_{0,1}+RY_{1,0}) \end{Bmatrix} \tag{A.4}$$

Also for $j=0,\ 1,\ 2$ and $\ell=0,\ 1$:

$$\begin{cases} \Lambda_{\ell,j}=\int_{-\frac{h}{2}}^{\frac{h}{2}}\lambda E\left[(1-\nu)\varepsilon_x^c+\nu(\varepsilon_\theta^c+\varepsilon_z^c)+(1+\nu)\alpha_T T\right]\left(1+\frac{z}{R}\right)^\ell z^j dz \\ I_{\ell,j}=\int_{-\frac{h}{2}}^{\frac{h}{2}}\lambda E\left[(1-\nu)\varepsilon_\theta^c+\nu(\varepsilon_x^c+\varepsilon_z^c)+(1+\nu)\alpha_T T\right]\left(1+\frac{z}{R}\right)^\ell z^j dz \\ Y_{\ell,j}=\int_{-\frac{h}{2}}^{\frac{h}{2}}\lambda E\left[(1-\nu)\varepsilon_z^c+\nu(\varepsilon_x^c+\varepsilon_\theta^c)+(1+\nu)\alpha_T T\right]\left(1+\frac{z}{R}\right)^\ell z^j dz \\ X_j=\int_{-\frac{h}{2}}^{\frac{h}{2}}\lambda E\left(1+\frac{z}{R}\right)z^j dz \\ \Upsilon_j=\int_{-\frac{h}{2}}^{\frac{h}{2}}\lambda E z^j dz \\ Z_j=\int_{-\frac{h}{2}}^{\frac{h}{2}}\lambda\frac{E}{R+z}z^j dz \end{cases} \tag{A.5}$$

Appendix B

$$\{F_c\} = \begin{Bmatrix} \left(D_0 + R\Gamma_{1,0}\right) \\ \dfrac{d}{dx}\left(R\Gamma_{1,1}\right) \\ -E_{0,0} \\ \left(-E_{0,1} - RH_{1,0}\right) \end{Bmatrix} \tag{B.1}$$

where for $j = 0,\ 1,\ 2$ and $\ell = 0,\ 1$:

$$\begin{cases} \Gamma_{\ell,j} = \int_{-\frac{h}{2}}^{\frac{h}{2}} \lambda E\left[\left(1-\nu\right)\dot{\varepsilon}_x^c + \nu\left(\dot{\varepsilon}_\theta^c + \dot{\varepsilon}_z^c\right)\right]\left(1+\dfrac{z}{R}\right)^\ell z^j dz \\ E_{\ell,j} = \int_{-\frac{h}{2}}^{\frac{h}{2}} \lambda E\left[\left(1-\nu\right)\dot{\varepsilon}_\theta^c + \nu\left(\dot{\varepsilon}_x^c + \dot{\varepsilon}_z^c\right)\right]\left(1+\dfrac{z}{R}\right)^\ell z^j dz \\ H_{\ell,j} = \int_{-\frac{h}{2}}^{\frac{h}{2}} \lambda E\left[\left(1-\nu\right)\dot{\varepsilon}_z^c + \nu\left(\dot{\varepsilon}_x^c + \dot{\varepsilon}_\theta^c\right)\right]\left(1+\dfrac{z}{R}\right)^\ell z^j dz \end{cases} \tag{B.2}$$

References

Afshin, A., Nejad, M. Z., Dastani, K. [2017] "Transient thermoelastic analysis of FGM rotating thick cylindrical pressure vessels under arbitrary boundary and initial conditions," *Journal of Computational Applied Mechanics* **48**(1), 15-26.

Daghigh, V., Daghigh, H., Loghman, A., Simoneau, A. [2013] "Time-dependent creep analysis of rotating ferritic steel disk using Taylor series and Prandtl–Reuss relation," *International Journal of Mechanical Sciences* **77**, 40-46.

Dehghan, M., Nejad, M. Z., Moosaie, A. [2016] "Thermo-electro-elastic analysis of functionally graded piezoelectric shells of revolution: Governing equations and solutions for some simple cases," *International Journal of Engineering Science* **104**, 34-61.

Fatehi, P., Nejad, M. Z. [2014] "Effects of material gradients on onset of yield in FGM rotating thick cylindrical shells," *International Journal of Applied Mechanics* **6**(4), 1450038.

Fesharaki, J. J., Loghman, A., Yazdipoor, M., Golabi, S. [2014] "Semi-analytical solution of time-dependent thermomechanical creep behavior of FGM hollow spheres," *Mechanics of Time-Dependent Materials* **18**(1), 41-53.

Ghannad, M., Nejad, M. Z., Rahimi, G. H. [2009] "Elastic solution of axisymmetric thick truncated conical shells based on first-order shear deformation theory," *Mechanika* **79**(5), 13-20.

Ghannad, M., Nejad, M. Z. [2010] "Elastic analysis of pressurized thick hollow cylindrical shells with clamped-clamped ends," *Mechanika* **85**(5), 11-18.

Ghannad, M., Nejad, M. Z., Rahimi, G. H., Sabouri, H. [2012] "Elastic analysis of pressurized thick truncated conical shells made of functionally graded materials," *Structural Engineering and Mechanics* **43**(1), 105-126.

Ghannad, M., Rahimi, G. H., Nejad, M. Z. [2013] "Elastic analysis of pressurized thick cylindrical shells with variable thickness made of functionally graded materials," *Composites Part B-Engineering* **45**(1), 388-396.

Gharibi, M., Nejad, M. Z., Hadi, A. [2017] "Elastic analysis of functionally graded rotating thick cylindrical pressure vessels with exponentially-varying properties using power series method of Frobenius," *Journal of Computational Applied Mechanics* **48**(1), 89-98.

Jabbari, M., Nejad, M. Z., Ghannad, M. [2015] "Thermo-elastic analysis of axially functionally graded rotating thick cylindrical pressure vessels with variable thickness under mechanical loading," *International Journal of Engineering Science* **96**, 1-18.

Jabbari, M., Nejad, M. Z., Ghannad, M. [2016] "Thermo-elastic analysis of axially functionally graded rotating thick truncated conical shells with varying thickness," *Composites Part B-Engineering* **96**, 20-34.

Kashkoli, M. D., Nejad, M. Z. [2014] "Effect of heat flux on creep stresses of thick-walled cylindrical pressure vessels," *Journal of Applied Research and Technology* **12**(3), 585-597.

Kashkoli, M. D., Nejad, M. Z. [2015] "Time-dependent thermo-elastic creep analysis of thick-walled spherical pressure vessels made of functionally graded materials," *Journal of Theoretical and Applied Mechanics* **53**(4), 1053-1065.

Kashkoli, M. D., Tahan, K. N., Nejad, M. Z. [2017a] "Time-dependent creep analysis for life assessment of cylindrical vessels using first order shear deformation theory," *Journal of Mechanics* **33**(4), 461-474.

Kashkoli, M. D., Tahan, K. N., Nejad, M. Z. [2017b] "Time-dependent thermomechanical creep behavior of FGM thick hollow cylindrical shells under non-uniform internal pressure," *International Journal of Applied Mechanics* **9**(6), 1750086 (26 pages).

Kassner, M. E. [2015] "Fundamentals of creep in metals and alloys," *Butterworth-Heinemann*, Oxford.

Kordkheili, S. H., Livani, M. [2013] "Thermoelastic creep analysis of a functionally graded various thickness rotating disk with temperature-dependent material properties," *International Journal of Pressure Vessels and Piping* **111**, 63-74.

Loghman, A., Ghorbanpour Arani, A., Aleayoub, S. [2011] "Time-dependent creep stress redistribution analysis of thick-walled functionally graded spheres," *Mechanics of Time-Dependent Materials* **15**(4), 353-365.

Loghman, A., Ghorbanpour Arani, A., Amir, S., Vajedi, A. [2010] "Magnetothermoelastic creep analysis of functionally graded cylinders," *International Journal of Pressure Vessels and Piping* **87**(7), 389-395.

Loghman, A., Moradi, M. [2017] "Creep damage and life assessment of thick-walled spherical reactor using Larson–Miller parameter," *International Journal of Pressure Vessels and Piping* **151**, 11-19.

Mantari, J., Granados, E. [2015] "A refined FSDT for the static analysis of functionally graded sandwich plates," *Thin-Walled Structures* **90**, 150-158.

Mazarei, Z., Nejad, M. Z., Hadi, A. [2016] "Thermo-Elasto-Plastic Analysis of Thick-Walled Spherical Pressure Vessels Made of Functionally Graded Materials," *International Journal of Applied Mechanics* **8**(4), 1650054.

Naumenko, K., Altenbach, H. [2007] "Modeling of creep for structural analysis," *Springer-Verlag Berlin Heidelberg*, Berlin.

Nayebi, A., Tirmomenin, A. and Damadam, M. [2015] "Elasto-plastic analysis of a functionally graded rotating disk under cyclic thermo-mechanical loadings considering continuum damage mechanics," *International Journal of Applied Mechanics* **7**(2), 1550026.

Nejad, M. Z., Rahimi, G. H. [2009] "Deformations and stresses in rotating FGM pressurized thick hollow cylinder under thermal load," *Scientific Research and Essays* **4**(3), 131-140.

Nejad, M. Z., Rahimi, G. H., Ghannad, M. [2009] "Set of field equations for thick shell of revolution made of functionally graded materials in curvilinear coordinate system," *Mechanika* **77**(3), 18-26.

Nejad, M. Z., Rahimi, G. H. [2010] "Elastic analysis of FGM rotating cylindrical pressure vessels," *Journal of the Chinese Institute of Engineers* **33**(4), 525-530.

Nejad, M. Z., Kashkoli, M. D. [2014] "Time-dependent thermo-creep analysis of rotating FGM thick-walled cylindrical pressure vessels under heat flux," *International Journal of Engineering Science* **82**, 222-237.

Nejad, M. Z., Fatehi, P. [2015] "Exact elasto-plastic analysis of rotating thick-walled cylindrical pressure vessels made of functionally graded materials," *International Journal of Engineering Science* **86**, 26-43.

Nejad, M. Z., Hoseini, Z., Niknejad, A., Ghannad, M. [2015a] "Steady-state creep deformations and stresses in FGM rotating thick cylindrical pressure vessels," *Journal of Mechanics* **31**(1), 1-6.

Nejad, M. Z., Jabbari, M., Ghannad, M. [2015b] "Elastic analysis of axially functionally graded rotating thick cylinder with variable thickness under non-uniform arbitrarily pressure loading," *International Journal of Engineering Science* **89**, 86-99.

Nejad, M. Z., Jabbari, M., Ghannad, M. [2015c] "Elastic analysis of FGM rotating thick truncated conical shells with axially-varying properties under non-uniform pressure loading," *Composite Structures* **122**, 561-569.

Nejad, M. Z., Hadi, A., Farajpour, A. [2017a] "Consistent couple-stress theory for free vibration analysis of Euler-Bernoulli nano-beams made of arbitrary bi-directional functionally graded materials," *Structural Engineering and Mechanics* **63**(2), 161-169.

Nejad, M. Z., Jabbari, M., Ghannad, M. [2017b] "A general disk form formulation for thermo-elastic analysis of functionally graded thick shells of revolution with arbitrary curvature and variable thickness," *Acta Mechanica* **228**(1), 215-231.

Rusinko, A. [2013] "Influence of annealing temperature in the course of mechanical-thermal treatment upon the steady-state creep rate of metals," *Journal of Mechanics* **29**(3), 535-538.

Sobhy, M. [2015] "Thermoelastic response of FGM plates with temperature-dependent properties resting on variable elastic foundations," *International Journal of Applied Mechanics* **7**(6), 1550082.

Sofiyev, A. [2011] "Thermal buckling of FGM shells resting on a two-parameter elastic foundation," *Thin-Walled Structures* **49**, 1304–1311.

Sofiyev, A. [2016] "Thermoelastic stability of freely supported functionally graded conical shells within the shear deformation theory," *Composite Structures* **152**, 74-84.

Sofiyev, A., Hui, D., Haciyev, V., Erdem, H., Yuan, G., Schnack, E., Guldal, V. [2017a] "The nonlinear vibration of orthotropic functionally graded cylindrical shells surrounded by an elastic foundation within first order shear deformation theory," *Composites Part B-Engineering* **116**, 170-185.

Sofiyev, A., Kuruoğlu, N. [2016] "The stability of FGM truncated conical shells under combined axial and external mechanical loads in the framework of the shear deformation theory," *Composites Part B-Engineering* **92**, 463-476.

Sofiyev, A., Zerin, Z., Kuruoglu, N. [2017b] "Thermoelastic buckling of FGM conical shells under non-linear temperature rise in the framework of the shear deformation theory," *Composites Part B-Engineering* **108**, 279-290.

Vlachoutsis, S. [1992] "Shear correction factors for plates and shells," *International Journal for Numerical Methods in Engineering* **33**(7), 1537-1552.